Acta Oceanol. Sin., 2024, Vol. 43, No. 4, P. 50–60
https://doi.org/10.1007/s13131-024-2341-8
http://www.aosocean.com
E-mail: ocean2@hyxb.org.cn

Structural features in the mid-southern section of the Kyushu–Palau Ridge based on satellite altimetry gravity anomaly

Feifei Zhang[1, 2, 4], Dingding Wang[1], Xiaolin Ji[3, 4], Fanghui Hou[2*], Yuan Yang[2], Wanyin Wang[1, 4, 5*]

[1] School of Geological Engineering and Geomatics, Chang'an University, Xi'an 710054, China

[2] Qingdao Institute of Marine Geology, China Geological Survey, Qingdao 266071, China

[3] Information and Navigation College, Air Force Engineering University, Xi'an 710077, China

[4] National Engineering Research Center of Offshore Oil and Gas Exploration, Beijing 100028, China

[5] Key Laboratory of Marine Geology and Environment, Institute of Oceanology, Chinese Academy of Sciences, Qingdao 266071, China

Received 31 October 2023; accepted 15 April 2024

Abstract

The Kyushu–Palau Ridge (KPR), an anti-S-shaped submarine highland at the center of the Philippine Sea Plate (PSP), is considered the residual arc of the Izu–Bonin–Mariana Island Arc, which retains key information about the cessation of the Western Philippine Basin (WPB) expansion and the Parece Vela Basin (PVB) breakup. Herein, using the new generation of satellite altimetry gravity data, high-precision seafloor topography data, and newly acquired ship-borne gravity data, the topographic and gravity characteristics of the KPR mid-southern section and adjacent region are depicted. The distribution characteristics of the faults were delineated using the normalized vertical derivative–total horizontal derivative method(NVDR-THDR) and the minimum curvature potential field separation method. The Moho depth and crustal thickness were inverted using the rapid inversion method for a double-interface model with depth constraints. Based on these results, the crust structure features in the KPR mid-southern section, and the "triangular" structure geological significance where the KPR and Central Basin Rift (CBR) of the WPB intersect are interpreted. The KPR crustal thickness is approximately 6–16 km, with a distinct discontinuity that is slightly thicker than the normal oceanic crust. The KPR mid-southern section crust structure was divided into four segments (S1–S4) from north to south, formed by the CBR eastward extension joint action and clockwise rotation of the PVB expansion axis and the Mindanao fault zone blocking effect.

Key words: structural features, satellite altimetry gravity data, Kyushu–Palau Ridge, Central Basin Rift, faults, Moho depth

Citation: Zhang Feifei, Wang Dingding, Ji Xiaolin, Hou Fanghui, Yang Yuan, Wang Wanyin. 2024. Structural features in the mid-southern section of the Kyushu–Palau Ridge based on satellite altimetry gravity anomaly. Acta Oceanologica Sinica, 43(4): 50–60, doi: 10.1007/s13131-024-2341-8

1 Introduction

The Kyushu–Palau Ridge (KPR) is an intraoceanic ridge in the central part of the Philippine Sea Plate (PSP). Trending nearly north–south (NS), the KPR divides the PSP into the West Philippine Basin (WPB) on the west side and the Shikoku–Parece Vela Basin (SPVB) on the east and is considered a remnant arc of the ancient Izu–Bonin–Mariana (IBM) arc basin system (Fig.1, Hilde and Lee, 1984; Park et al., 2009; Lallemand and Arcay, 2021). Because the ridge and its surrounding area record the information on plate tectonic movements in different geological historical periods, they can help elucidate the formation and evolution of plate subduction and intraoceanic arcs.

Hall et al. (1995) suggested that the collision between the Indian-Australian plate and the Eurasian Plate caused the change of stress field, triggering the subduction of the ancient Pacific Plate to the PSP. Stern (Stern, 2004; Stern and Gerya, 2018) considered the KPR as a typical autonomous subduction induced by the subsidence of the Pacific lithosphere along the transition fault/fracture zones. Taylor and Goodliffe (2004) argued that the tectonic distributions of the KPR and WPB are almost orthogonal, hindering the subduction process. Based on the latest multichannel reflection seismic profiles and drilling data, Hou et al. (2022) concluded that subduction along the ancient IBM arc was initiated by a far-field effect of the Indo–Asian collision and was accompanied by lateral propagation and a continuous extrusion stress field. Therefore, the initiation mechanism of plate subduction in the KPR has not been resolved in the theory of plate tectonics.

The crustal structure and tectonic evolution of the KPR have been the focus of attention. From 2004 to 2008, Japan began conducting a series of seismic surveys on the KPR that characterized the lithosphere structures of the northern section of the ridge and compared the northern and southern sections of the ridge to de-

Foundation item: 'Research on Deep Structural Differences between Potential Oil-rich Depressions in Offshore basins of China Sea' from the scientific and technological project of CNOOC Research Institute Co., Ltd., under contract No.CCL2021RCPS0167KQN; 'Resource Potential, Accumulation Mechanism and Breakthrough Direction of Potential Oil-rich Depressions in Offshore China Sea', under contract No. 220226220101; the Project of China Geological Survey under contract No. DD20191003; the National Natural Science Foundation of Shandong Province of China under contract No. ZR2022MD047.
*Corresponding author, E-mail: houfanghui3993@163.com; wwy7902@chd.edu.cn

limit the outer continental shelf of Japan (Nishizawa et al., 2007, 2016; Ishizuka et al., 2011). Nishizawa et al. (2007) studied the crust of the KPR from 15°N to 21°N using seafloor seismic data, and Ishizuka et al. (2011) summarized the crustal structures in the north and south sections of the KPR. The topography, crustal structure, and sedimentary features of the KPR have also been extensively studied by Chinese researchers (Zhang et al., 2012; Yang et al., 2021; Song et al., 2021; Shang et al., 2021; Hou et al., 2022; Wei et al., 2022).

Despite extensive studies on the KPR, some problems have not been properly resolved. First, in most previous studies, crystal structures have been inferred from a small number of seismic refraction/reflection profiles and few drilling data (Nishizawa et al., 2007, 2016; Park et al., 2009; Zhang et al., 2012; Ishizuka et al., 2011). The lack of accurate, full-coverage geophysical data has limited our understanding of the fine tectonic sedimentary features and crust–mantle structure of the KPR and its adjacent areas. Since the 1970s, satellite altimetry has enabled the determination of marine gravity fields at high resolution over large areas. Satellite altimetry gravity data has been widely applied in studies on regional structure, oil and gas exploration, and models of the Earth's gravity (Jin and Gao, 2001; Chao et al., 2002; Ning et al., 2016; Ji et al., 2019a), providing useful information on marine regional structures.

Based on the comprehensive scientific survey data newly obtained by the Qingdao Institute of Marine Geology (China Geological Survey, 2018–2022) and the new generation of satellite altimetry gravity data (SSV 29.1, Sandwell et al., 2013, 2014, 2021), this study reports the structural features of the mid-southern sections of the KPR and its surrounding areas (indicated by the purple solid box in Fig. 1). The faults distribution and Moho features are inferred from the seafloor topographic and gravity anomaly features. The study discusses the segmentation features and tectonic movement of the mid-southern sections of the KPR. The integrated interpretation result provides basic geophysical information on the tectonic evolution of the KPR and the delimitation of the continental shelf.

2 Geological setting

The PSP is among the largest marginal seas in the western Pacific Region. Located at the confluence of the Eurasian Plate, the Australian Plate, and the Pacific Plate (Fig. 1), the PSP is surrounded by several deep-sea trenches. From north to south, the eastern edge accommodates the Izu–Bonin Trench, Mariana Trench, Yap Trench, Palau Trench, and Ayu Trench. At the side of the western edge reside the Nankai Trough, Ryukyu Trench, Manila Trench, and Philippine Trench (Wu et al., 2013).

With an approximate length and width of 2 750 km and 90 km, respectively, the KPR follows an "anti-S" trajectory through the Philippine Sea. The KPR comprises the Kyushu Ride and Palau Ridge and separates the PSP into the WPB on the west and the SPVB on the east. The water depth at the top of the ridge ranges from 1 500 m to 4 000 m, and the slopes on the east and west sides are asymmetric (Li et al., 2000). The KPR can be divided into three segments with varying tectonic trends, seafloor topography characteristics, and crustal structures. In the northern segment of the KPR (north of 21°N), the total crustal thickness is approximately 13 km (Ishihara and Koda, 2007; Yamashita et al., 2007). In the middle segment of the KPR (mainly at 15°–21°N), the crust thickness varies from 8 km to 20 km, which is slightly thicker than the thickness of the sea basin on both sides of the ridge (Ishihara and Koda, 2007; Hou et al., 2022). The crustal thickness of the southern segment of the KPR (located south of

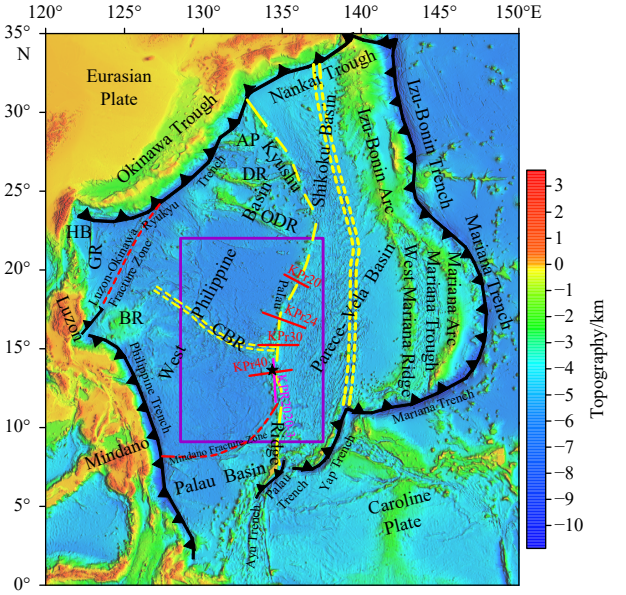

Fig. 1. Tectonic setting of the Philippine Sea (Wu et al., 2016). The elevation data are taken from Smith and Sandwell (1997). The double yellow dashed lines indicate the active and inactive spreading centers and the single dashed yellow line denotes the Kyushu–Palau Ridge (KPR). The purple boxes delineate the study ranges. Solid red and pink lines indicate the positions of the deep reflection seismic profiles (Nishizawa et al., 2007; Wei et al., 2022). Dashed red lines indicate the fracture zones and transform faults. AP: Amami Plateaul; BR: Benham Rise; CBR: Central Basin Rift; DR: Daito Ridge; GR: Gagua Ridge; HB: Huatung Basin; ODR: Oki-Daito Ridge.

15°N) is generally between 6 km and 12 km(Wei et al., 2022). The mid-south sections of the KPR have a complex crustal structure and remain poorly characterized owing to a lack of geophysical exploration.

The formation and evolution of the KPR have been explained based on various mechanisms. The consensus view is a close relationship between the tectonic evolution of the KPR and the evolution of the PSP. At around 29 Ma, the PSP began moving northwestward (3.5 cm/a), the IBM trench split eastward, and the SPVB began expanding in the near east–west (EW) direction (Kobayashi, 2004; Yamashita et al., 2007). The KPR then detached from the ancient IBM island arc and became a residual arc (Kobayashi, 2004; Nishizawa et al., 2007; Park and Hori, 2009). Considering the segmented crustal structure of the KPR, Zhang et al. (2012) proposed that cracking of the KPR began at both ends and slowly extended to the middle, gradually separating the KPR from the IBM island arc. From the ages of volcanic rocks in different sections of the KPR, Hou et al. (2022) deduced that the KPR becomes gradually younger toward the KPR–CBR intersection.

3 Data and methods

3.1 *Data*

This study uses the V29.1 version satellite altimetry gravity data, which is equivalent to the free-air gravity anomaly obtained by Sandwell et al. (2013, 2014, 2021) and the V19.1 topographical data obtained by Smith and Sandwell (1997); both datasets are 1′ × 1′ grids. According to the latest research results, the mean square

error between the satellite altimetry gravity data of V29.1 and ship-borne gravity data is less than 1×10^{-5} m/s^2 (Zhang and Zhang, 2005; Sandwell et al., 2013, 2014, 2021; Luo et al., 2022; Zhang et al., 2023), which can meet the demand of geological structural research on the 1:500 000 scale. The high-resolution ship-borne gravity data in the study area were obtained in the 2018–2022 period and collected from the Qingdao Institute of Marine Geology, China Geological Survey. The accuracy of the ship-borne gravity data is within 1×10^{-5} m/s^2.

Furthermore, the water depth, sediment thickness, sediment density, and Moho depth constraints were collected for related data processing. The sediment thicknesses were taken from a dataset of total sediment thicknesses in the world's oceans (GlobSed) with a grid spacing of 5′ (Straume et al., 2019). The density of the sedimentary in this study uses the density of the global seabed reported by Graw et al. (2021), which is obtained using a random forest machine learning method on a grid spacing of 5′. The Moho depth data (grid spacing 1°) are taken from LITHO1.0 (Pasyanos et al., 2014) with a grid spacing of 1°.

3.2 *Methods*

The gravity anomaly comprehensively reflects the density in homogeneities from the surface to the deep earth. When interpreting the geological structure based on the gravity anomaly, the interference information should be eliminated to obtain the information related to the geological structure. The present study adopts the following technologies for processing the satellite altimetry gravity data.

(1) To improve the data accuracy, we used the minimum curvature method (Ji et al., 2015, 2019b) to suppress the noise of the satellite altimetry gravity data and ship-borne gravity data. Based on the linear correlation between the satellite altimetry gravity data and ship-borne gravity data (Zhang et al., 2023), we linearly regressed (Zhang et al., 2007; Hu et al., 2014) the satellite altimetry gravity data against the ship-borne gravity data in the study area.

(2) To eliminate the influence of topography and seawater layer on the gravity anomaly, we obtained the Bouguer gravity anomaly by applying the generalized topographic correction method (Lei, 1984) to the satellite altimetry gravity data. The average density of the crust was assumed as 2.67×10^3 kg/m^3; the density of seawater and the Bouguer correction radius were 1.03×10^3 kg/m^3 and 166.7 km, respectively.

(3) Both sides of the linear structures (including the geological faults and the boundaries of different tectonic units) show laterally heterogeneous rock densities in most cases. Gravity anomalies of the faults and tectonic boundaries are usually characterized by gravity anomaly gradient zone or distortion. The deep faults and tectonic boundaries were identified using the normalized vertical derivative–total horizontal derivative (NVDR–THDR) method (Wang et al., 2009, 2021).

(4) To accurately obtain the abnormalities caused by geological bodies, the residual information must be extracted from the total gravity anomalies. The residual Bouguer gravity anomaly was derived from Bouguer gravity anomaly using the superposition step iterative in situ of minimum-curvature method (Ji et al., 2015, 2019b) with a step size of 11 and an iteration number of 36.

(5) The Moho interface between the crust and the upper mantle is also a density interface, so it is considerably useful for probing deep structures. Based on the Bouguer gravity anomaly data, the gravity effect of the sedimentary layer was evaluated using the fast forward modeling method in a double-interface model (Wang and Pan, 1993). The Moho depth in the mid-southern section of the KPR was determined using the fast-inversion method in the double-interface model (Wang and Pan, 1993) under the constraints of the LITHO1.0 point data at the Moho depth.

4 Results

4.1 *Seafloor topography and gravity anomaly*

The water depth in the study area ranges from 303.9 m to 7 760 m, and the seabed morphological features differ among the tectonic units (WPB, PVB, and KPR; Fig. 2).

The KPR, which occupies the middle of the Philippine Sea Basin, is arc-shaped with a shallow water depth. From north to south, the KRP can be divided into five sections (S1–S4) separated by boundaries near latitudes of 17° N, 14° N, and 10° N. The direction and topographic characters of each segment are different, where S1 is narrow and trends NNE, S2 is nearly SN-trending and approximately 61 km wide from east to west, S3 is NNW-trending and many NE- and NEE-trending subridges are formed in an echelon arrangement, and S4 is a continuous island-arc topography extending southward from SN- to NE-trending. There are three topographic gaps distributed on the KPR, which make its topography discontinuous. The seafloor topography at both sides of the KPR, which is characterized by sharp and steep scarps, is presumably formed through early proto-arc separation (Nishizawa et al., 2016).

The west side of the KPR is the WPB, which is divided into two symmetrical basin regions by the NW-trending CBR. The CBR is a NW-trending rift valley with a maximum water depth of approximately 7 500 m. Based on its morphological features, the CBR

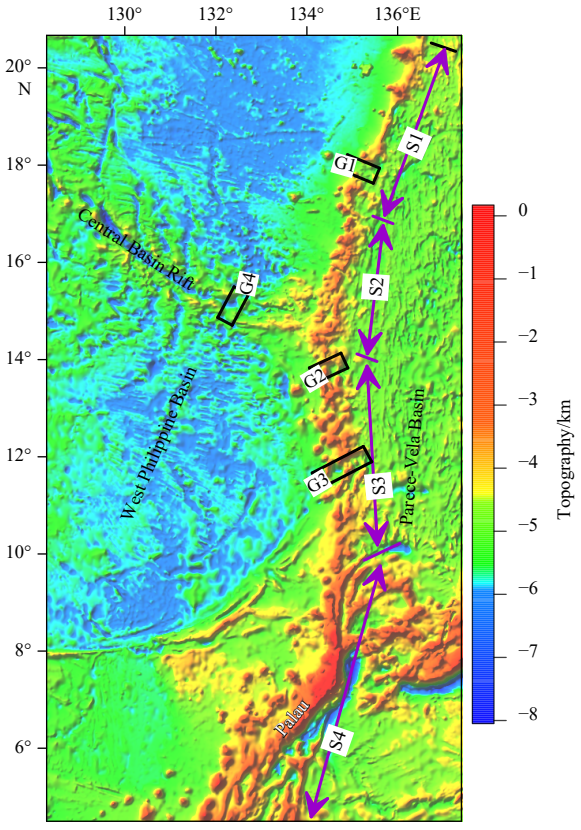

Fig. 2. Seafloor topography map of the study area with data from http:www.ngdc.noaa.gov/mgg/global/global.html. The KPR is divided into four segments (S1–S4). The black rectangles (G1–G4) represent topographic gaps, which disconnect KPR and CBR.

can be approximately divided into eastern and western segments bounded by an SN-trending depression at 132.5° E longitude (G4 in Fig. 2). The western segment of the CBR is narrow (approximately 20 km wide) and nearly SN-trending alternating ridges and troughs appear at both sides. The eastern segment of the CBR is located east of G4 in a triangular terrain, which is narrow in the west and wide in the east. Two large topographic highlands comprising small ridges and seamounts are developed on the north and south sides of the CBR. The east side of the KPR is the PVB, with a seabed topography characterized by alternately distributed ridges and grooves trending nearly SN.

4.2 *Gravity anomaly*

Within the KPR and its adjacent area (Fig. 3a), the amplitude of the gravity anomaly ranges from -68.698×10^{-5} m/s^2 to 127.30×10^{-5} m/s^2, and that of the Bouguer gravity anomaly (Fig. 3b) ranges from -240.40×10^{-5} m/s^2 to 431.60×10^{-5} m/s^2.

The gravity anomaly of the KPR is distinctly segmented. The gravity anomaly in the S1 segment is NNE-trending and characterized by a narrow and long high-gravity anomaly zone. In the S2 segment, the gravity anomaly is nearly SN-trending, and the width of the gravity anomaly is wider than that of the S1 segment. The gravity anomaly between S1 and S2 segments in the KPR is rendered discontinuous by a NW-trending high-gravity anomaly belt at a latitude of nearly 17°N. The gravity anomaly between latitudes of 14.5°N and 16°N is influenced by the CBR structure and protrudes westward, forming an EW-trending gravity anomaly. The gravity anomaly in the S3 segment is NNW-trending. The satellite altimetry shows a discontinuously distributed gravity anomaly in the S3 segment characterized by multiple NNE-trending high- or low-amplitude gravity anomalies arranged in an echelon pattern. Both sides of the KPR are gravity anomaly gradient zones, steep in the west and gentle in the east. The S4 segment is located in the Palau area, with a continuous, narrow, and high-gravity anomaly belt. The northern segment is narrow and nearly SN-trending, and the southern segment is NE-trending. The gravity anomaly between S3 and S4 has obvious dislocation at a latitude of nearly 10°N, which is speculated to be a deep fault.

The gravity anomaly in the WPB is an NS symmetrical distribution gravity anomaly area bounded by an NW-trending CBR anomaly zone. The CBR anomaly zone is characterized by a low anomaly in the middle and high anomalies on both sides. Several near-SN-trending high-gravity anomaly belts are distributed on the north and south sides of the CBR. The eastern part of the CBR gravity anomaly belt is connected with the S2 section of the KPR, and the anomaly belt east of the longitude of 132°E becomes nearly EW-trending.

4.3 *Division and distribution of faults*

The faults in the study area were systematically identified through the NVDR–THDR of gravity anomalies and residual gravity anomalies. The area contains 11 main structural boundary faults (F_1–F_9, F_S and F_N), 3 segmented faults in the KPR (F_{K1}–F_{K3}), 7 transform faults in the WPB (TF_1–TF_7) and several secondary faults. The boundary faults and transform faults are well reflected on the NVDR–THDR map (Fig. 4a), and the secondary faults are mainly divided by discontinuities or distortions of residual Bouguer gravity anomalies (Fig. 4b).

The trends and lengths of the faults were counted (Table 1), and the fault trends were plotted as a rose diagram (Fig. 5). Most of the faults are near-SN-, NW-, and NNE-trending. The dominant trend is near-SN-trending (mainly including the KPR fault system and the transition faults in the WPB), and the total length

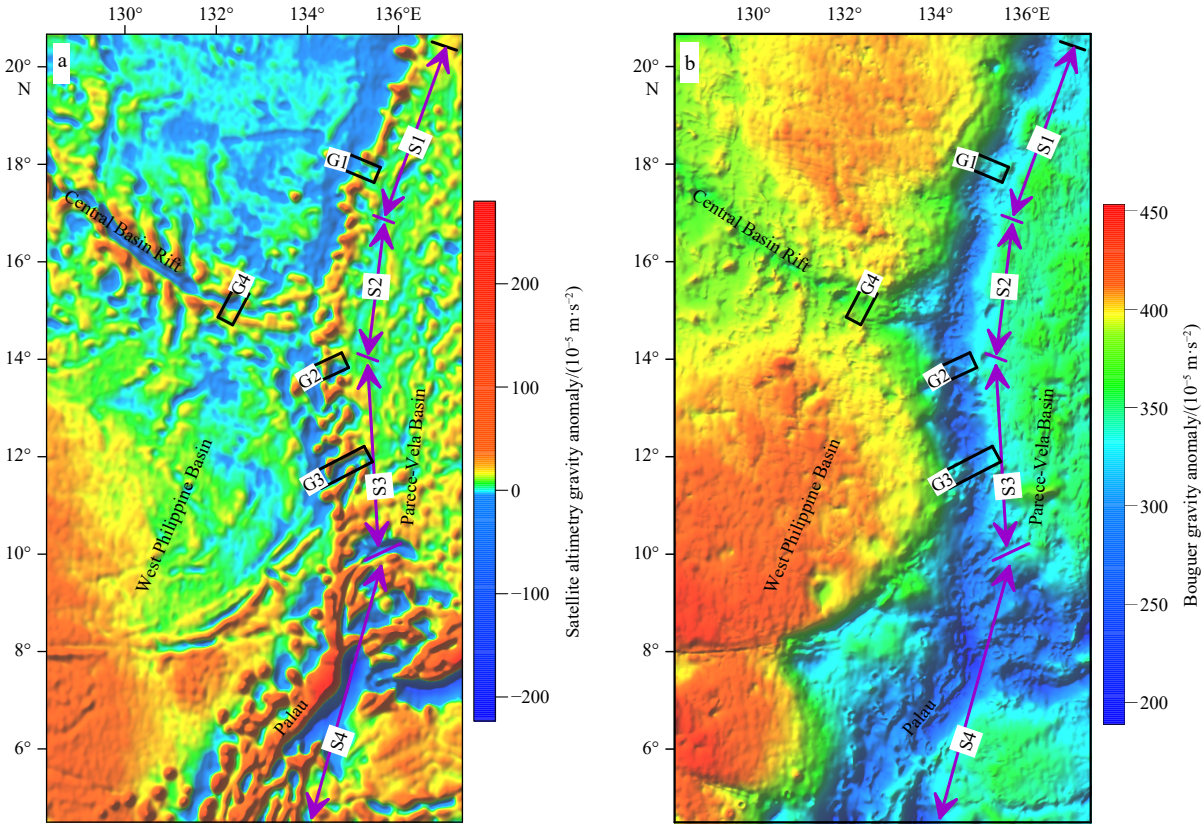

Fig. 3. Gravity anomaly maps of the study area. a. Satellite altimetry gravity anomaly (free-air gravity anomaly). b. The Bouguer gravity anomaly.

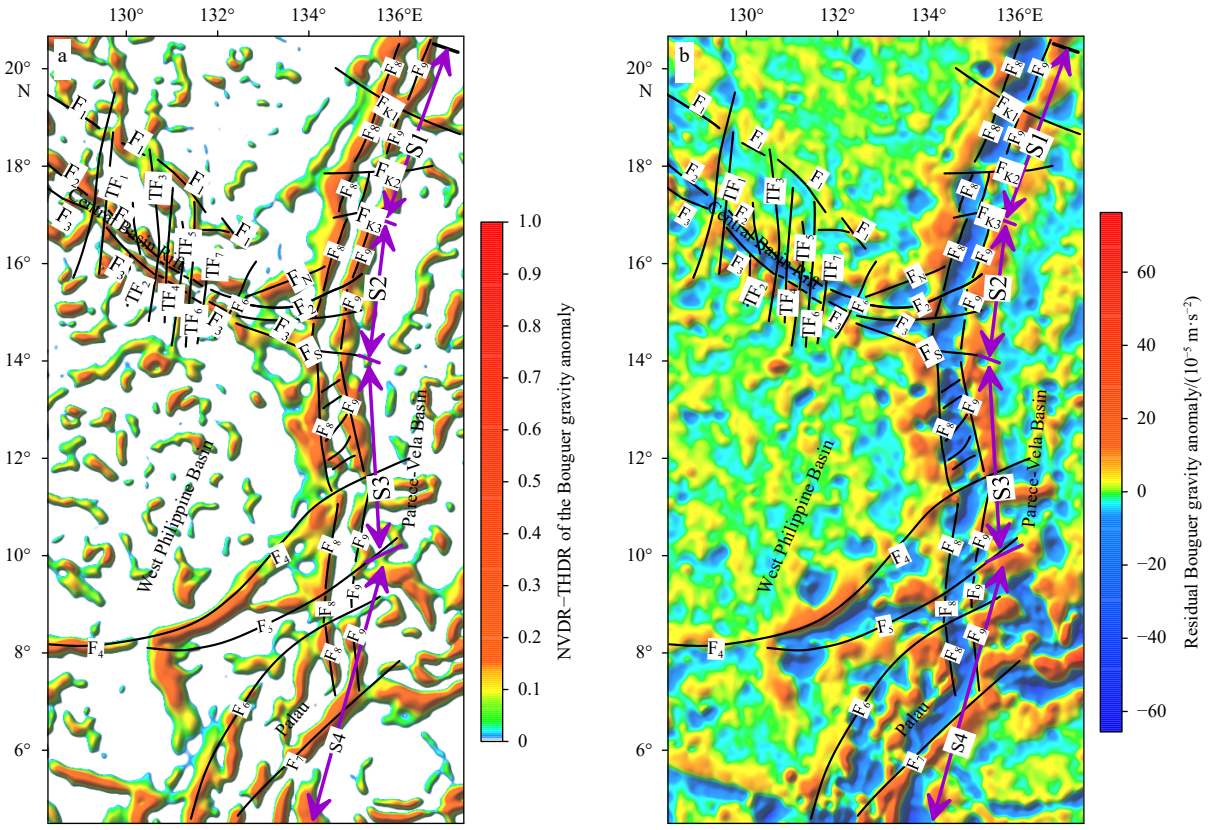

Fig. 4. Distribution maps of the faults in the study area. a. NVDR-THDR results of the Bouguer gravity anomaly. b. The residual Bouguer gravity anomaly.

Table 1. Features of the faults in the mid-southern KPR and adjacent areas

Fault	Trend	Length/km	Mutually broken relationship	Location
F_1	NW	680	broken by the TF_1, TF_2 and TF_3	located in the north of the CBR, the boundary between the northern basin and the central rift
F_2	NW	950	broken by the TF_1–TF_2 and misplaces the F_4 and F_5	located in the north of the CBR, the northern boundary of the central rift
F_3	NW	1 000	broken by the TF_1–TF_2, and misplaces the F_4 and F_5	located in the north of the CBR, the southern boundary of the central rift
F_4	NEE	970	misplaces the F_8 and F_9	located in the north of the Palau Basin and corresponds to the Mindano Fracture Zone
F_5	NEE	645	misplaces the F_8 and F_9	
F_6	NE	690		located in the west of the Palau island
F_7	NE	510		located in the east of the Palau island
F_8	near-SN	1 560	broken by the F_{K1}, F_{K2}, F_{K3}, F_2, F_3, F_4, F_5 and F_s	located in the west of the KPR, the western boundary of the KPR
F_9	near-SN	1 565	broken by the F_{K1}, F_{K2}, F_{K3}, F_2, F_3, F_4, F_5 and F_s	located in the east of the KPR, the eastern boundary of the KPR
F_N	NE	200		located in the north of the eastern section of CBR
F_S	NW	300	misplaces the F_8 and F_9	located in the south of the eastern section of CBR and extends through KPR to PVB
F_{K1}	NW	325		
F_{K2}	near-EW	230	misplaces the F_8 and F_9	segmental fault of KPR
F_{K3}	near-EW	120		
TF_1		430		
TF_2		330		
TF_3		390		
TF_4	near-SN	310	misplaces the F_1, F_2 and F_3	distributed in the CBR as transform faults
TF_5		280		
TF_6		330		
TF_7		200		

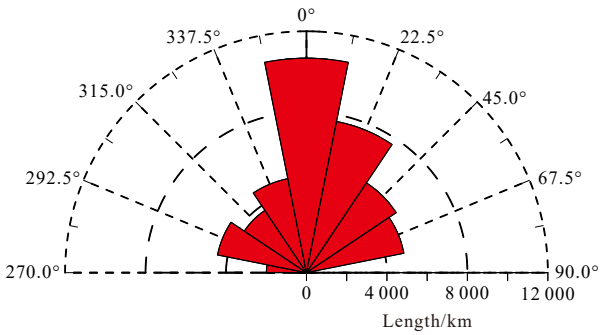

Fig. 5. Rose diagram of faults strikes in the study area.

of the near-SN-trending faults exceeds 10 500 km.

4.4 *Calculation result of the Moho depth and Crustal thickness*

The variation trends of the Moho depth (Fig. 6a) and crustal thickness (Fig. 6b) in the study area reflect the deep structural features of different structural units. A three-dimensional gravity model of the PSP (Ishihara and Koda, 2007) yielded a little thicker crust in the KPR and CBR (8–16 km) and a thin crust in the WPB and PSB. The same features were obtained in our inversion results.

The Moho depth of the KPR is approximately 11–18 km, and the crust thickness is about 6–16 km. In the mid-southern section of the KPR, the Moho is a narrow strip-shaped crustal depression with a deep contour gradient zone on both sides, being steep in the west and gentle in the east. The Moho depth shows distinct segmentation features consistent with the segmentation features of the topography and gravity anomaly. From north to south, it is divided into four sections with different crustal-distribution features.

The WPB and PVB are sea-basin areas with relatively shallow Moho depths (8–10 km), consistent with the typical Moho depths in global sea basins. The Moho depth is slightly deeper in the PVB than in the WPB, consistent with the results of P-wave velocity (Vp) models of KPr24 and KPr40 seismic profiles (Figs 8 and 9; Nishizawa et al., 2016). The CBR is the center of the inactive basin expansion and was the site of an active volcanic eruption. Therefore, the Moho depth is approximately 10–11 km thicker in the CBR than in the sea basin.

5 Discussion

5.1 *Analysis of segmented structural features of the mid-southern section of the KPR*

Based on OBS profiles across the KPR (Ishihara and Koda, 2007; Nishizawa et al., 2007, 2016), the crustal thickness of the KPR was inferred as 8–23 km, with a relatively thin crust and thick middle and upper crusts. However, other studies showed that the KPR lacks a middle crust (Zhang et al., 2012; Calvert, 2011), and the crustal thickness is about 6–12 km (Wei et al., 2022). It is slightly thicker than normal oceanic crust such as WPB and PVB, but it is much thinner than mature island crust such as the IBM arc.

This study obtained the Moho depth and the crustal thickness in the mid-southern section of KPR using gravity data. The inversion results show that the crustal thickness of KPR is approximately 6–16 km with a distinct discontinuity, indicating pronounced segmentation features. The mid-southern section can also be subdivided into four segments separated by boundaries

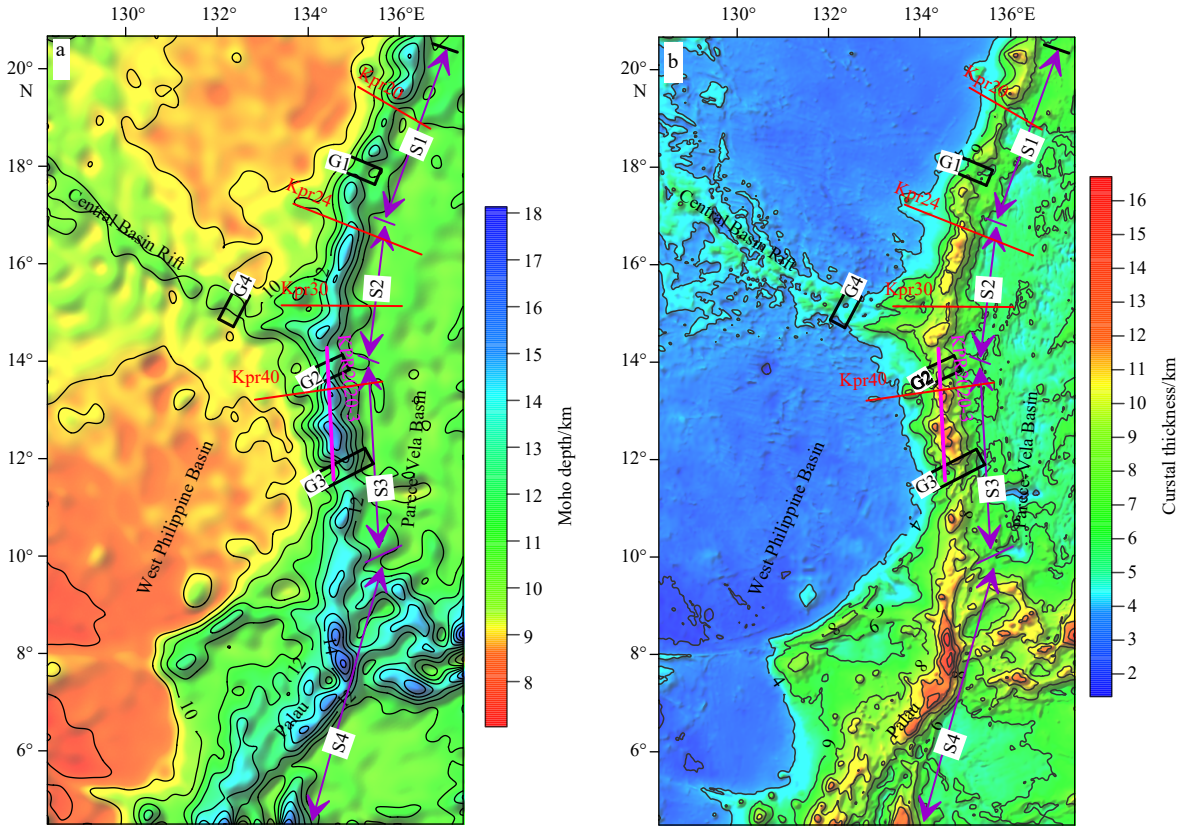

Fig. 6. Inversion results of Moho depth and crustal thickness in the study area. a. Moho depth map. b. Crustal thickness map.

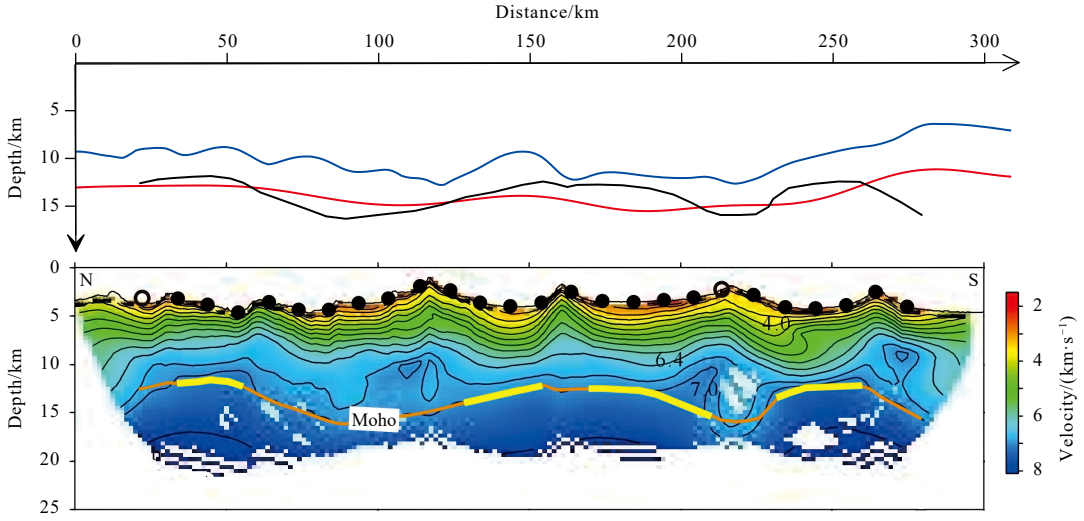

Fig. 7. Comparison between the gravity inversion result and Vp models for line KPR2020-3 (Wei et al., 2022). The solid blue line is crustal thickness, the solid red line is Moho depth using gravity inversion, and the solid black line is Moho depth obtained by deep reflection/refraction seismic data.

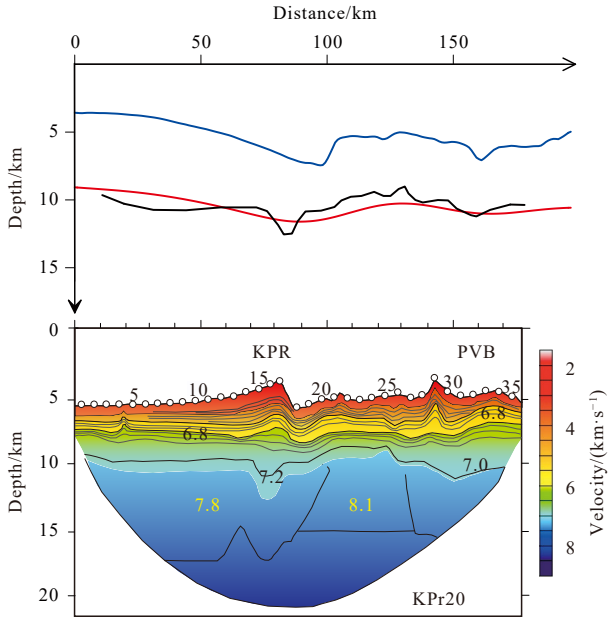

Fig. 8. Comparison between the gravity inversion result and Vp models for line KPr20 (Nishizawa et al., 2016). The solid blue line is crustal thickness, the solid red line is Moho depth using gravity inversion, and the solid black line is Moho depth obtained by deep reflection/refraction seismic data. KPR: Kyushu–Palau Ridge; PVB: Parece Vela Basin.

near the latitudes of 17°N, 14°N and 10°N.

We compared the Moho depths obtained via gravity inversion for one wide-angle seismic profile KPR2020-3 (Fig. 7) from Wei et al. (2022) and four typical seismic profiles (Figs 8–10, KPr20, KPr24, KPr30, and KPr40) selected from Nishizawa et al. (2016). The trends the crust derived from gravity inversion corresponded well with the Vp results, showing that the crust of KPR is thicker than the neighboring basin crusts of the WPB and PVB to the west and east, consistent with the result of KPR2020-3 (Fig. 7). However, the Moho depth is 2–5 km shallower than the Vp model of KPr24, KPr30, and KPr40.

The mid-section of KPR presents four discontinuous subridges and can be divided into two segments (S1 and S2) with different topographical and gravity features. The S1 segment includes three discontinuous narrow subridges with a discontinuous Bouguer anomaly and thinned crust between the subridges, showing independent anomaly traps. Therefore, it was inferred that the continuity of the crust of the S1 segment is disrupted by the NE-trending faults of F_{K1} and F_{K2}. The Vp model of the KPr20 profile (Fig. 8) shows a narrow and notably thickened crust in the KPR region. The crustal-thickness inversion results based on the gravity anomaly show the KPR crustal thickness is approximately 6–7 km, which is less thicker than the crustal thickness of the WPB and PVB. On the crust thickness map (Fig. 6b), the crustal thickness of the S1 segment is the thinnest in the mid-southern section of KPR, and the crustal changes are asymmetrically distributed on both sides of the ridge. The crust-thickness gradient is steep on the west side, where the crust is thinner, and gentle on the east side, where the crust is thicker.

The S2 segment is distinctly wider in the EW direction than the S1 segment, and the strike changes to nearly SN. The ridges on the north and south sides of the F_{K3} fault are obviously dislocated, and the gravity anomalies and crustal structures clearly differ between S1 and S2. The crustal thickness of the S2 segment is 8–10 km, which has a little thicker crust than S1 and symmetrically distributed changes on the east and west sides of the ridge. The trending of crust is consistent with the Vp model of KPr24 (Fig. 9), but the thickness is thinner than the KPr24. A special crustal feature appears on the S2 segment located at the CBR–KPR junction. The Vp model of KPr30 (Nishizawa et al., 2016) revealed a thicker crust in the WPB than in the PVB (Fig. 10). Furthermore, the crustal thickness map shows a triangular crustal-thickening area at the CBR–KPR junction where the crust is 2–3 km thicker than in the neighboring areas. The seismic profile reveals two sets of sediment cover layers of different thicknesses and different sources in the CBR–KPR junction (Hou et al.,2022). The lower sequence is mostly volcanic material derived from the volcanism of the KPR, showing a continuous thickening in the direction of the sea ridge (Hou et al., 2022). In summary, the middle section of the KPR (segments S1 and S2) presents a typical segmentation feature with clear discontinuity in topo-

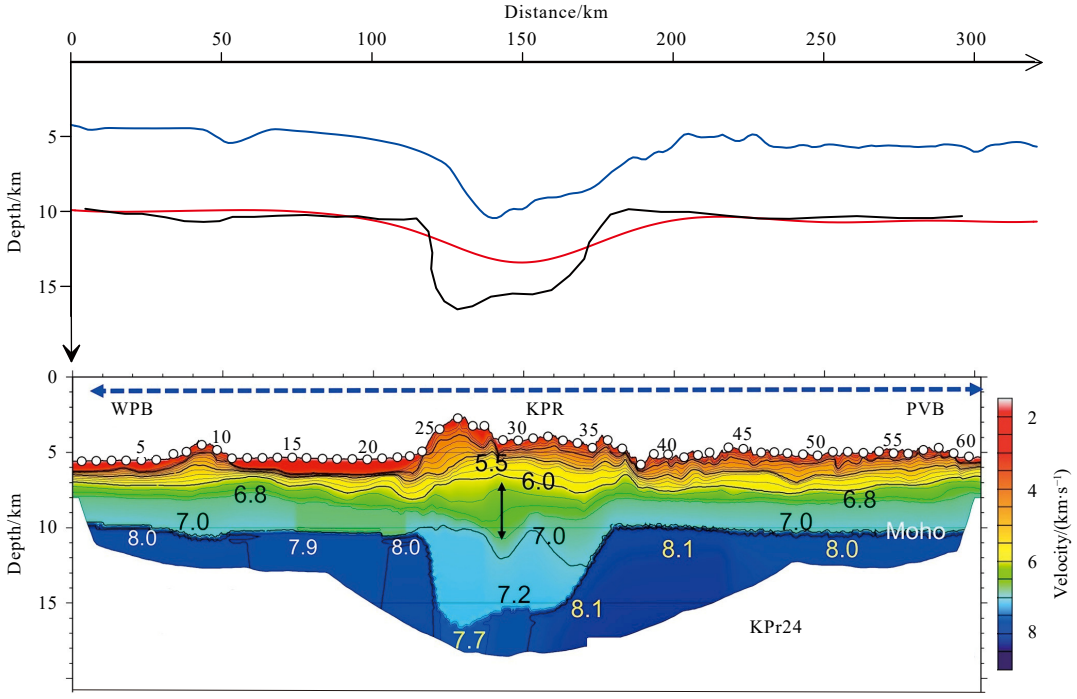

Fig. 9. Same as Fig. 7 but for KPr24 (Nishizawa et al., 2016). WPB: West Philippine Basin; KPR: Kyushu–Palau Ridge; PVB: Parece Vela Basin.

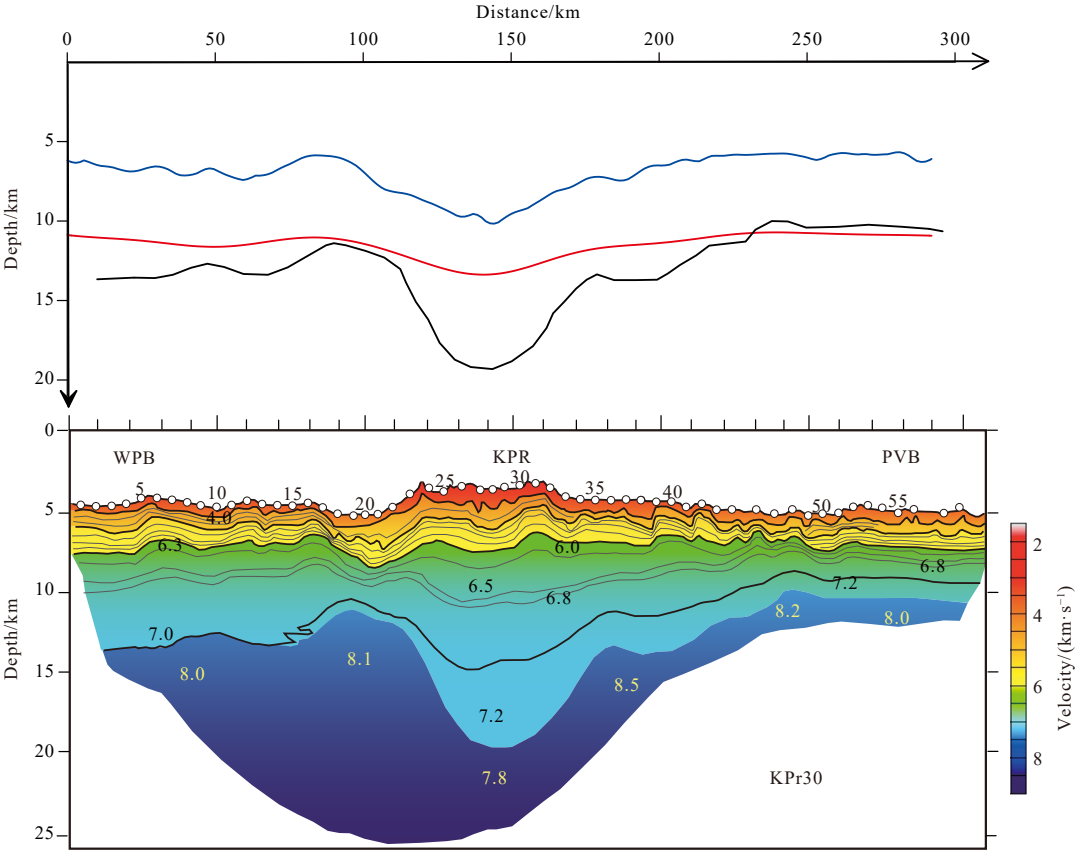

Fig. 10. Same as Fig. 7 but for KPr30 (Nishizawa et al., 2016). WPB: West Philippine Basin; KPR: Kyushu–Palau Ridge; PVB: Parece Vela Basin.

graphy, gravity anomaly, and crustal structure.

The S3 segment of the KPR presents a discontinuous seafloor topography and gravity anomaly with NNE-trending echelon arrangement on the plane. The fault system also shows a number of NE-trending faults arranged in an echelon pattern. This tectonic feature is consistent with that of the PVB and is possibly related

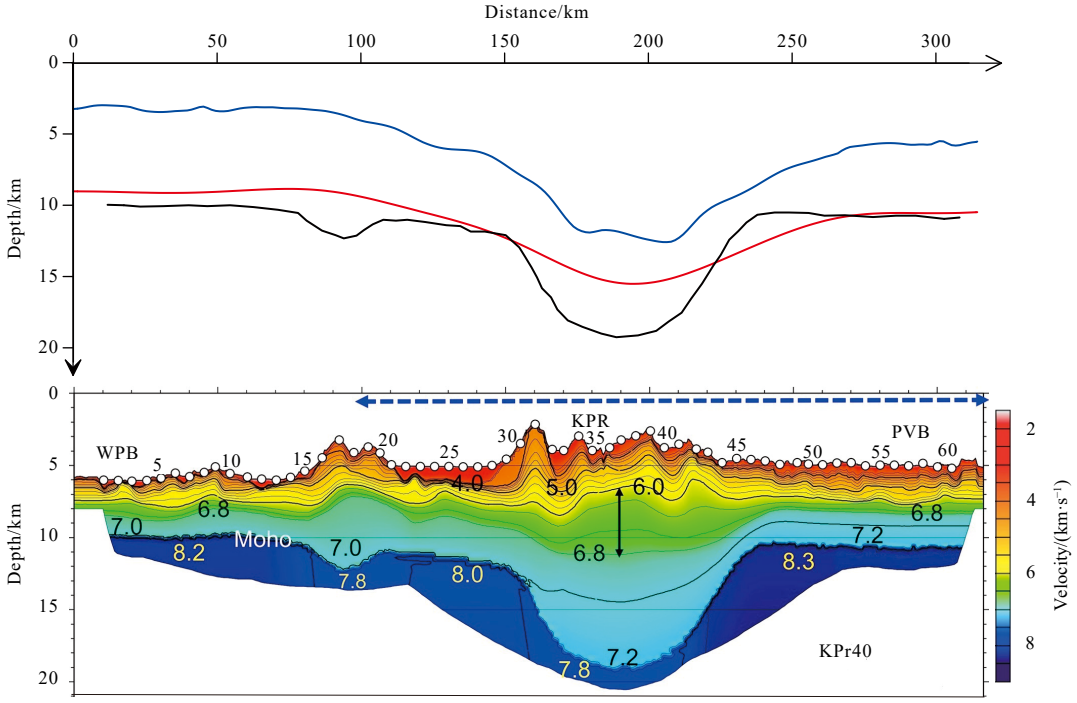

Fig. 11. Same as Fig.7 but for line KPr40 (Nishizawa et al., 2016). WPB: West Philippine Basin; KPR: Kyushu–Palau Ridge; PVB: Parece Vela Basin.

to the cutting of the transform faults during the formation of the PVB. However, no NE-trending echelon arrangement appears in the Bouguer gravity anomaly and Moho depth map, indicating no disruption to the Moho during this process. The crustal thickness of the S3 segment is about 8–12 km, which is close to the result of KPR2020-3 (Fig. 7) but thinner than the crustal thickness of KPr40 (Fig. 11).

The S4 segment located south of 10°N is different from S1–S3, which are mainly manifested in the continuous characteristics of topography and gravity anomalies and the obvious thickening of the crust. On the crust thickness map (Fig. 6b), the S4 crustal thickness (~10–16 km) is thicker than the other segments. According to the fault distribution and crustal characteristics, it was inferred that the Mindanao Fracture Zone (F_4 and F_5) north and south side ridges have different structural characteristics.

The tectonic grain of the mid-southern section of the KPR noticeably varies along the ridge from north to south, which changes from NNE to near-SN to NE. Why does the trend of the ridge change? At approximately 19 Ma, the expansion axis of the PVB rotated clockwise, and the splitting direction of the KPR changed from the original near-EW direction to the SW–NE direction (Zhang et al., 2007). The eastward extension of the CBR near 14.5° N affected the rotation of the expansion axis of the PVB on the KPR, causing inconsistent stress directions between the north and south ridges and consequent changes in ridge direction. The KPR north of 14.5°N is NNE-trending, consistent with the direction of the transform faults in the PVB, and is marginally affected by the tectonic stress of the transform fault. Conversely, the KPR south of 14.5°N is NNW-trending and obliquely intersects the transform faults of the PVB. Therefore, under the tectonic stress of the transform faults, the southern section of the KPR was cut into an echelon arrangement of subridges. Furthermore, the Mindano fault zone blocked the expansion action of the PVB, resulting in no expansion of the island arc near Palau. Therefore, the north and south sides of the Mindano fault zone have completely different crustal characteristics.

5.2 *Structural feature analysis of the KPR - CBR*

The CBR is an ancient spreading axis that has ceased its activity in the center of the WPB. Based on ocean drilling results and comparisons of the magnetic anomaly bands (26–13 magnetic stripes) in the CBR, the spreading center became inactive at 33 Ma (Hou et al., 2022). After the tectomagmatic activity ceased, the basement sediment was mainly sourced from the KPR on the east side. Therefore, the seafloor topography and gravity anomaly features on both sides of the CBR mainly reflect the processes of the last stage of tectonic activity, including the transformation of the expansion direction of the WPB and distribution of the transform faults. The CBR is orthogonal to the KPR near 15° N, forming a pseudo triple-junction structure. Previously, it was believed that the KPR–CBR triple junction evolved from the trench–trench–rift triple point (Deschamps et al., 2002; Deschamps and Lallemand, 2002; Okino and Fujioka, 2003; Shang et al., 2021)

As the CBR extended eastward, the KPR–CBR intersection formed a unique “triangular” structure with obvious seafloor topography and gravity anomaly features. The tectonic influence ranged from 14.5°N to 16°N and from 132°E to 135°E. The KPR and CBR converged to form a triangle that is wide in the east and narrow in the west. On the seafloor of the KPR–CBR is a symmetrical distribution of triangular positive topography on both sides of the CBR. The gravity anomaly of the KPR–CBR indicates a narrow high-gravity anomaly zone with a dominant distribution of high-gravity anomaly traps, indicating that both sides of the CBR are high-density magmatic rocks extended by the boundary faults of the CBR.

The shallow drill core, which is located on the ridge at the KPR–CBR junction (identified by star symbols in Fig. 1), reveals a set of calcareous cemented slump conglomerates containing abundant paleontological fossils and volcanic breccias. Accord-

ing to the Cenozoic age of detrital zircons, at least three discontinuous arc volcanic activities (at approximately 41 Ma, 36 Ma, and 31 Ma) occurred in the KPR (Hou et al., 2022), respectively, providing a source of magmatic rock migration. The topography and gravity anomaly morphology at the KPR–CBR are characteristically "wide in the east and narrow in the west," indicating that the magma gradually weakened while its distribution range narrowed during the migration process. The migration ended near 132.5° E. The increase in the amount of the volcanic material substantially thickened the crust at the KPR–CBR intersection over a range consistent with the "triangular" structure.

Four EW-extended super-crustal faults appear in the "triangle" structure of the KPR–CBR. Faults F_2 and F_3 are the boundary faults of CBR, which might extend eastward to break the KPR and provide migration channels for magmatic rocks. Faults F_N and F_S are the boundary faults of the "triangle" structure, which control the migration range of magmatic rocks. The magmatic rock migrates westward along the boundary fault zone on both sides of the CBR, forming a long strip of high-gravity anomaly. Taking F_2 and F_3 as the boundary faults, the structural trend and fault combinations clearly differ between the north and south sides of the KPR.

In summary, we inferred that the CBR extended eastward below the KPR, disrupting the original structure of the KPR and segmenting the ridge between 14.5°N and 16°N. The orthogonal structure of the KPR–CBR affected the direction of tectonic movement during the splitting process of the KPR, leading to different structural features in the north and south sections. Because rock-age information is lacking in the CBR, the geological period of magmatic rock migration along the faults cannot be obtained. Therefore, the evolution process between the KPR and the CBR is uncertain, and their interactions cannot be elucidated until the relevant evidence and constraints become known.

6 Conclusions

Based on satellite altimetry gravity data, this study investigated the large-scale structural features of the mid-southern section of the KPR and its adjacent sea areas. The main faults in the study area were identified, and the Moho depth was calculated. The fault system, Moho depth and structural features of the mid-southern section of the KPR were analyzed and discussed. The conclusions of this study are summarized below.

(1) Eleven boundary faults of tectonic units, seven transition faults, and three segmented faults were inferred in the KPR. The plane distribution of the fault systems in the study area and their interrelationships were preliminarily inferred from gravity data in the mid-southern KPR and the adjacent sea area. The study area is dominated by the nearly SN-trending KPR fault system and the NW-trending CBR fault system. The boundary faults of the CBR extended eastward, disrupting the boundary faults of the KPR near 14.5° N and playing a key role in the tectonic segmentation of the KPR.

(2) The mid-southern section of the KPR shows distinct segmentation features and can be divided into four segments from north to south. The seafloor topography, gravity anomaly, and crustal thickness of the ridge are obviously discontinuous. The S1–S3 crustal thickness is 6–12 km, which is slightly thicker than normal oceanic crust, implying that the KPR mid-southern section is a thick oceanic crust. Meanwhile, the S4 crustal thickness is 8–16 km and is obviously thickened. The S4 crustal properties are different from those of the other KPR sections located north of the Mindanao fault zone.

(3) The tectonic evolution of the mid-southern section of the KPR is closely related to the evolution of the CBR and PVB. The expansion axis of the PVB rotated clockwise, altering the splitting direction of the KPR; meanwhile, the CBR orthogonal to the KPR and extended eastward, disrupting the original structure of the KPR and causing different structural features of the ridges on the north and south sides of the KPR–CBR. Simultaneously, the magmatic rocks migrated westward along the KPR–CBR, forming a triangular crustal-thickening area between 14.5°N and 16°N.

(4) This study provides an interpretation of the tectonic evolution of the KPR. It also provides geophysical technical support for structural research in deep-sea areas. Our results are limited to the description and inference of seafloor topography, gravity anomaly, and fault system features in the study area; the evolution model was not discussed in depth.

References

Chao Dingbo, Yao Yunsheng, Li Jiancheng, et al. 2002. Interpretaion on the tectonics and characteristics of altimeter-derived gravity anomalies in China South Sea. Geomatics and Information Science of Wuhan University (in Chinese), 27(4): 343–347

Calvert A J. 2011. The seismic structure of island arc crust. In: Brown D, Ryan P D, eds. Arc-Continent Collision Berlin, Heidelberg: Springer, 87–119

Deschamps A, Lallemand S. 2002. The West Philippine Basin: an Eocene to Early Oligocene back arc basin opened between two opposed subduction zones. Journal of Geophysical Research: Solid Earth, 107(B12): 2322

Deschamps A, Okino K, Fujioka K. 2002. Late amagmatic extension along the central and eastern segments of the West Philippine Basin fossil spreading axis. Earth and Planetary Science Letters, 203(1): 277–293, doi: 10.1016/S0012-821X(02)00855-5

Graw J H, Wood W T, Phrampus B J. 2021. Predicting global marine sediment density using the random forest regressor machine learning algorithm. Journal of Geophysical Research: Solid Earth, 126(1): e2020JB020135, doi: 10.1029/2020JB020135

Hall R, Ali J R, Anderson C D, et al. 1995. Origin and motion history of the Philippine Sea Plate. Tectonophysics, 251(1–4): 229–250, doi: 10.1016/0040-1951(95)00038-0

Hilde T W C, Lee C S. 1984. Origin and evolution of the west Philippine Basin: a new interpretation. Tectonophysics, 102(1–4): 85–104, doi: 10.1016/0040-1951(84)90009-X

Hou Fanghui, Qin Ke, Lu Kai, et al. 2022. Tectono-sedimentary characteristics and subduction initiation in the middle Kyushu-Palau Ridge and adjacent basins: a comprehensive study of multichannel seismic reflection profiles. Marine Geology & Quaternary Geology (in Chinese), 42(5): 187–198

Hu Zhengan, Zhang Chunguan, Ren Zusong, et al. 2014. Calculation of the Satellite Altimetric bouguer gravity anomaly based on regression analysis. Journal of Yangtze University (Natural Science Edition) (in Chinese), 11(1): 21–23

Ishihara T, Koda K. 2007. Variation of crustal thickness in the Philippine Sea deduced from three-dimensional gravity modeling. Island Arc, 16(3): 322–337, doi: 10.1111/j.1440-1738.2007.00593.x

Ishizuka O, Taylor R N, Yuasa M, et al. 2011. Making and breaking an island arc: a new perspective from the Oligocene Kyushu-Palau arc, Philippine Sea. Geochemistry, Geophysics, Geosystems, 12(5): Q05005

Ji Xiaolin, Wang Wanyin, Du Xiangdong, et al. 2019a. Tectonic division by gravity and magnetic anomaly data of salt-bearing basins, south-central section of West Africa. Chinese Journal of Geophysics (in Chinese), 62(4): 1502–1514

Ji Xiaolin, Wang Wanyin, Qiu Zhiyun. 2015. The research to the minimum curvature technique for potential field data separation. Chinese Journal of Geophysics (in Chinese), 58(3): 1042–1058

Ji Xiaolin, Wang Wanyin, Qiu Zhiyun. 2019b. Parameter choose experimental research to the minimum curvature technique potential field data separation method. Progress in Geophysics (in Chinese), 34(4): 1441–1452

Jin Xianglong, Gao Jinyao. 2001. The satellite altimetry gravity field

and the geodynamic feature in the West Pacific. Marine Geology & Quaternary Geology (in Chinese), 21(1): 1–6
Kobayashi K. 2004. Origin of the Palau and Yap trench-arc systems. Geophysical Journal International, 157(3): 1303–1315, doi: 10.1111/j.1365-246X.2003.02244.x
Lallemand S, Arcay D. 2021. Subduction initiation from the earliest stages to self-sustained subduction: insights from the analysis of 70 Cenozoic sites. Earth-Science Reviews, 221: 103779, doi: 10.1016/j.earscirev.2021.103779
Lei Shoumin. 1984. Calculation of generalized topographic and isostatic gravity corrections. Marine Geology & Quaternary Geology (in Chinese), 4(1): 101–111
Li Changzhen, Li Naisheng, Lin Meihua. 2000. Terrain features of the Philippine sea. Marine Sciences (in Chinese), 24(6): 47–51
Luo Zhicai, Zhong Bo, Zhou Hao, et al. 2022. Progress in determining the Earth's gravity field model by satellite gravimetry. Geomatics and Information Science of Wuhan University (in Chinese), 47(10): 1713–1727
Ning Jinsheng, Wang Zhengtao, Chao Nengfang. 2016. Research status and progress in international next-generation satellite gravity measurement missions. Geomatics and Information Science of Wuhan University (in Chinese), 41(1): 1–8
Nishizawa A, Kaneda K, Katagiri Y, et al. 2007. Variation in crustal structure along the Kyushu-Palau Ridge at 15–21°N on the Philippine Sea plate based on seismic refraction profiles. Earth, Planets and Space, 59(6): e17–e20
Nishizawa A, Kaneda K, Oikawa M. 2016. Crust and uppermost mantle structure of the Kyushu-Palau Ridge, remnant arc on the Philippine Sea Plate. Earth, Planets and Space, 68(1): 30
Okino K, Fujioka K. 2003. The Central Basin Spreading Center in the Philippine Sea: structure of an extinct spreading center and implications for marginal basin formation. Journal of Geophysical Research: Solid Earth, 108(B1): 2040
Park J O, Hori T, Kaneda Y. 2009. Seismotectonic implications of the Kyushu - Palau Ridge subducting beneath the westernmost Nankai forearc. Earth, Planets and Space, 61(8): 1013–1018
Pasyanos M E, Masters T G, Laske G, et al. 2014. LITHO1.0: an updated crust and lithospheric model of the Earth. Journal of Geophysical Research: Solid Earth, 119(3): 2153–2173, doi: 10.1002/2013JB010626
Sandwell D, Garcia E, Soofi K, et al. 2013. Toward 1-mGal accuracy in global marine gravity from CryoSat-2, Envisat, and Jason-1. The Leading Edge, 32(8): 892–899, doi: 10.1190/tle32080892.1
Sandwell D T, Harper H, Tozer B, et al. 2021. Gravity field recovery from geodetic altimeter missions. Advances in Space Research, 68(2): 1059–1072, doi: 10.1016/j.asr.2019.09.011
Sandwell D T, Müller R D, Smith W H F, et al. 2014. New global marine gravity model from CryoSat-2 and Jason-1 reveals buried tectonic structure. Science, 346(6205): 65–67, doi: 10.1126/science.1258213
Shang Luning, Li Panfeng, Du Runlin, et al. 2021. Structural characteristics of the KPR-CBR triple-junction inferred from gravity and magnetic interpretations, Philippine Sea Plate. China Geology, 4(4): 541–552, doi: 10.31035/cg2021089
Smith W H F, Sandwell D T. 1997. Global sea floor topography from satellite altimetry and ship depth soundings. Science, 277(5334): 1956–1962, doi: 10.1126/science.277.5334.1956
Song Weiyu, Liu Yanan, Hu Bangqi, et al. 2021. Landform classification for the Philippine Sea Based on DEM data. Marine Geology & Quaternary Geology (in Chinese), 41(1): 192–198
Stern R J. 2004. Subduction initiation: spontaneous and induced. Earth and Planetary Science Letters, 226(3–4): 275–292, doi: 10.1016/S0012-821X(04)00498-4
Stern R J, Gerya T. 2018. Subduction initiation in nature and models: a review. Tectonophysics, 746: 173–198, doi: 10.1016/j.tecto.2017.10.014
Straume E O, Gaina C, Medvedev S, et al. 2019. GlobSed: updated total sediment thickness in the world's oceans. Geochemistry, Geophysics, Geosystems, 20(4): 1756–1772
Taylor B, Goodliffe A M. 2004. The West Philippine Basin and the initiation of subduction, revisited. Geophysical Research Letters, 31(12): L12602
Wang Wanyin, Pan Zuoshu. 1993. Fast solution of forward and inverse problems for gravity field in a dual interface model. Geophysical Prospecting for Petroleum (in Chinese), 32(2): 81–87, 123
Wang Wanyin, Pan Yu, Qiu Zhiyun. 2009. A new edge recognition technology based on the normalized vertical derivative of the total horizontal derivative for potential field data. Applied Geophysics, 6(3): 226–233, doi: 10.1007/s11770-009-0026-x
Wang Dingding, Wang Wanyin, Zhu Yingjie, et al. 2021. Extraction methods and application of feature points of edge recognition for potential field. Chinese Journal of Geophysics (in Chinese), 64(4): 1401–1411
Wei Xiaodong, Ding Weiwei, Ruan Aiguo, et al. 2022. Crustal structure and variation along the southern part of the Kyushu-Palau Ridge. Acta Oceanologica Sinica, 41(1): 50–57, doi: 10.1007/s13131-021-1979-8
Wu Shiguo, Fan Jianke, Dong Dongdong. 2013. Discussion on the tectonic division of the Philippine Sea Plate. Chinese Journal of Geology (in Chinese), 48(3): 677–692
Wu J, Suppe J, Lu Renqi, et al. 2016. Philippine Sea and East Asian plate tectonics since 52 Ma constrained by new subducted slab reconstruction methods. Journal of Geophysical Research: Solid Earth, 121(6): 4670–4741, doi: 10.1002/2016JB012923
Yamashita M, Tsuru T, Takahashi N, et al. 2007. Fault configuration produced by initial arc rifting in the Parece Vela Basin as deduced from seismic reflection data. Island Arc, 16(3): 338–347, doi: 10.1111/j.1440-1738.2007.00594.x
Yang Huiliang, Wei Jia, Li Panfeng, et al. 2021. Characteristics of the stratigraphic architectures of the shallow sections in deep sea basin on both sides of Kyushu - Palau ridge. Marine Geology & Quaternary Geology (in Chinese), 41(1): 14–21
Zhang Jie, Li Jiabiao, Ding Weiwei. 2012. Reviews of the study on crustal structure and evolution of the Kyushu-Palau ridge. Advances in Marine Science (in Chinese), 30(4): 595–607
Zhang Feifei, Wang Hao, Zhang Yimi, et al. 2023. Accuracy analysis of satellite altimetry gravity data in the Western Pacific Area. Geomatics and Information Science of Wuhan University (in Chinese),). https://doi.org/10.13203/j.whugis20220429 [2023/-05/-26]
Zhang Minghua, Zhang Jiaqiang. 2005. Resolution of modern satellite altimetric gravity anomaly and its application to marine geological survey. Geophysical & Geochemical Exploration (in Chinese), 29(4): 295–298,303
Zhang Chunguan, Zhang Minghua, An Yulin. 2007. The negative correlation correction between gravity anomaly and topography of Tibetan Plateau. Geophysical & Geochemical Exploration (in Chinese), 31(3): 236–238